JTEIN: Jurnal Teknik Elektro Indonesia, Vol. 6, No. 2, pp. 145-158, 2025
e-ISSN 2723-0589

# Frequency-Domain Analysis of a Single-Machine Infinite-Bus Control System Equipped with a Power System Stabilizer Using the Backtracking Search Algorithm

**Heru Dibyo Laksono[1*], Suci Maretta Salim[1]**

[1] Department of Electrical Engineering,Faculty of Engineering, Universitas Andalas, Padang, INDONESIA

*Corresponding Author, email : herudibyolaksono@eng.unand.ac.id



**Abstract**

The SMIB model with a PSS optimized through the BSA is employed in this research to investigate the improvement of electrical power system stability. The performance of both open-loop and closed-loop systems is evaluated through frequency domain analysis. System stability and control efficacy are evaluated through key metrics such as gain and phase margins, resonance peaks, and robustness parameters. Simulation outcomes reveal marked enhancements in the optimized configuration. In particular, the phase margin is negative, suggesting instability, and the open-loop gain margin is infinite in the absence of PSS. The introduction of the BSA-optimized PSS leads to a gain margin of 27.96 dB and an infinite phase margin, which satisfy the design specifications. The closed-loop bandwidth surpasses 7.11 rad/s, with the resonance peak maintained between 1.0 and 1.5, allowing for prompt transient response and robust performance. This study underscores BSA's effectiveness in fine-tuning PSS parameters, yielding enhanced system stability and attenuation of low-frequency oscillations. These results contribute to the development of advanced robust control methodologies in power systems.

**Keywords**: Single Machine Infinite Bus (SMIB); Power System Stabilizer (PSS); Backtracking Search Algorithm (BSA); system stability; Domain Frequency Analysis

## 1. Introduction

The rapid advancement of technology in the digital era has underscored the critical role of electrical energy as a fundamental requirement across various human activities. Electrical energy is delivered through interconnected power system networks, the stability of which is essential to ensure reliable and efficient operation [1]. The implementation and modeling of power generation systems in the Single Machine Infinite Bus (SMIB) framework have become increasingly relevant in addressing the demand for system stability and operational efficiency in modern power grids. Synchronous generators, serving as the primary sources of electricity in power plants, require robust and accurate modeling to capture their dynamic interactions with the infinite bus through transmission lines [2], [3]. The SMIB model offers a simplified yet effective representation used in power system studies to analyze the dynamic behavior and stability of a single generator connected to an infinite bus, which emulates a large power system with constant voltage and frequency. This model is particularly useful for investigating the generator's response to disturbances such as faults and load fluctuations, which can induce frequency and rotor angle oscillations, potentially leading to system instability [4], [5]. To mitigate these oscillations, the Power System Stabilizer (PSS) is employed as a crucial component designed to enhance damping of electromechanical oscillations. The PSS, typically structured using lead-lag

compensators and optimized via techniques such as damping torque analysis, is vital in suppressing low-frequency oscillations that may hinder power transfer capabilities and compromise system stability. The SMIB model provides a foundational framework for the design, analysis, and validation of PSS strategies, offering valuable insights into system dynamics and facilitating the development of effective control mechanisms to ensure stable and efficient operation of power systems [6], [7].

In addition, the use of Power System Stabilizers (PSS) is common for damping low-frequency oscillations and enhancing dynamic stability by optimizing the frequency and rotor angle response, thereby minimizing system overshoot and reducing settling time [8]. Lead-lag Power System Stabilizers are critical components in power systems, specifically designed to improve system stability by mitigating low-frequency oscillations (LFO) that may arise due to disturbances within the network. These stabilizers function by adjusting the phase and gain of control signals to enhance the damping characteristics of the power system. The configuration of the lead-lag compensator parameters is crucial for effective PSS operation, as it directly influences the system's ability to suppress oscillations. Traditional methods for configuring these parameters can be inefficient and suboptimal, prompting the development of automated techniques using tools such as MATLAB to optimize phase response across a range of frequencies [9].

Stability analysis in the frequency domain is a crucial aspect in ensuring the reliability and efficiency of various control systems, particularly in the context of power generation and distribution. A study by Wang et al. highlights the importance of impedance-based analysis in grid-connected inverters, emphasizing how control parameters—such as voltage loop control settings—can significantly influence subsynchronous oscillations, which are critical to the successful integration of renewable energy sources into the power grid [10]. Frequency-domain stability analysis using Bode plots serves as a critical approach for evaluating the stability of diverse systems, including power electronics and multi-inverter-fed power systems. The use of Bode plots is particularly advantageous due to their ability to visually represent system dynamics and stability margins in an intuitive and informative manner [11]. In the analysis of the Single Machine Infinite Bus (SMIB) system within the frequency domain—particularly with regard to rotor angle and angular velocity—considerations of open-loop and closed-loop configurations as well as robustness analysis are involved. Rotor angle stability is of paramount importance for maintaining synchronous operation [12]. The implementation of Power System Stabilizers (PSS) in SMIB systems has been shown to optimize frequency and rotor angle responses, minimize overshoot, and improve settling time, thereby enhancing the system's ability to maintain stability under load variations [5]. A comprehensive stability assessment—encompassing both steady-state and transient conditions—is essential to ensure stable power system operation, and this necessitates accurate modeling of various components such as synchronous machines and transmission lines [13]. Within the SMIB framework, the use of nonlinear observer-based controllers has been demonstrated to improve system stability by effectively rejecting model parameter uncertainties and unmeasured input disturbances, thereby providing a systematic design approach that balances transient response and robustness [14].

Various optimization techniques have been explored to enhance the performance of Power System Stabilizers (PSS) in such systems. For instance, the Dynamic Crow Search Algorithm (DCSA) has been applied to optimize PSS parameters, demonstrating improved convergence and robustness in damping oscillations under varying operating conditions [15]. Similarly, the Chaotic Quasi-Oppositional Differential Search Algorithm (CQODSA) has been employed for optimal PSS tuning, proving effective across a wide range of loading scenarios [16]. Furthermore, the Grey Wolf Optimizer (GWO) has been utilized in fuzzy logic-based PSS designs to achieve faster settling times and improved damping of low-frequency oscillations when compared to conventional stabilizers [17].

The Backtracking Search Algorithm (BSA) is a contemporary stochastic optimization technique that has been effectively applied to various complex engineering and numerical optimization problems. It is distinguished by its ability to explore global optima through a population-based approach, leveraging memory capabilities and a simple structure to produce high-quality solutions [18]. BSA has emerged as a powerful optimization method used across a range of applications in power system modeling. It has proven highly effective in addressing complex problems such as Optimal Reactive Power Flow (ORPF) and Load Frequency Control (LFC). In the context of ORPF, BSA has been applied to systems incorporating High Voltage Direct Current (HVDC) links and shunt capacitor banks, demonstrating superior performance in minimizing voltage drops and enhancing system efficiency compared to alternative methods [19].

Moreover, BSA's robustness and efficiency have been highlighted in geophysical applications, where it has successfully resolved gravity anomaly inversions, offering a viable alternative to other global optimizers such as Particle Swarm Optimization [20]. The algorithm's precision, convergence capability, and stability have been further validated in solving nonlinear equations across various physical systems, where it has shown competitive performance relative to state-of-the-art techniques [21].

In this research, the impact of modification Power System Stabilizer (PSS) parameters on the dynamic response of a Single Machine Infinite Bus (SMIB) system is investigated to ascertain the frequency domain response and robustness of the SMIB control system using the Backtracking Search Algorithm (BSA). The significance of this research lies in enhancing the understanding of how PSS influences the dynamic behavior of SMIB systems, which is crucial for identifying potential risks and performance issues in power network functionality—particularly under varying load conditions and disturbances. Furthermore, the study contributes to the development of insights that support the optimal configuration of PSS, thereby advancing control system strategies for modern electric power networks.

## 2. Methods

The research begins by designing a model related to the elements in the SMIB configuration integrated with the PSS using mathematical modeling. The transfer function of the SMIB system is derived from the SMIB state equation.

$$\Delta\dot{x} = A\Delta x + B\Delta u \quad (1)$$

$$\Delta y = C\Delta x + D\Delta u \quad (2)$$

The transfer function is defined as the ratio between the Laplace transform of the output and input under zero initial conditions; thus, $x(0)$ is assumed to be zero. From this, the following is obtained:

$$\frac{Y(s)}{U(s)} = G(s) = C(sl - A)^{-1}B + D \quad (3)$$

The input matrix B is constructed under the assumption that a mechanical torque input is applied, and the corresponding system response is analyzed. This perturbation results in a change in acceleration, which can be expressed as:

$$\alpha = \frac{\Delta T_m}{M} \quad (4)$$

Where α denotes acceleration. An increase in load causes the electrical power output to rise, leading to a deceleration that reduces the rotor speed. Conversely, a decrease in load results in a drop in electrical power, causing acceleration and an increase in rotor angular velocity. In this model, the B matrix is determined based on an assumed disturbance equivalent to 10% of the mechanical torque, applied from 1.0 to 1.1 seconds, and the corresponding system response is observed. The C matrix, representing the output, yields the rotor angle, angular velocity, internal voltage, excitation voltage, and control signal. Meanwhile, the D matrix is considered null in this configuration

JTEIN: Jurnal Teknik Elektro Indonesia, Vol. 6, No. 2, pp. 145-158, 2025
e-ISSN 2723-0589



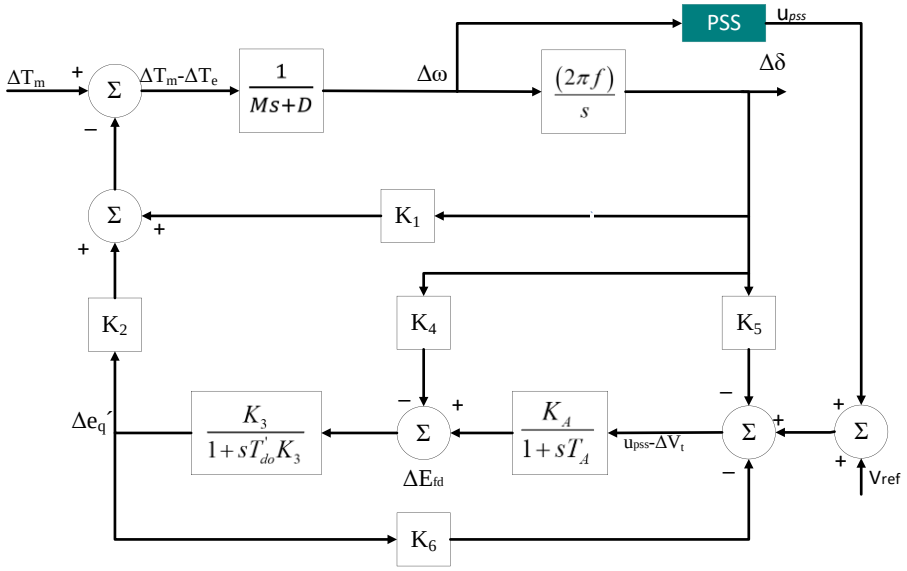


**Figure 1: SMIB Block Diagram with PSS.**

The matrix elements of the system can be written as follows

$$\begin{bmatrix} \Delta\dot{\delta} \\ \Delta\dot{\omega} \\ \Delta\dot{e}'_q \\ \Delta\dot{E}_{FD} \\ \dot{x}_5 \\ \dot{u}_E \end{bmatrix} = [A_c] \begin{bmatrix} \Delta\delta \\ \Delta\omega \\ \Delta e'_q \\ \Delta E_{FD} \\ x_5 \\ u_E \end{bmatrix} + [B][\Delta T_m] \quad (5)$$

Where,

$$[A_c] = \begin{bmatrix} 0 & \omega_b & 0 & 0 & 0 & 0 \\ -\frac{K_1}{M} & -\frac{D}{M} & -\frac{K_2}{M} & 0 & 0 & 0 \\ -\frac{K_4}{T'_{do}} & 0 & -\frac{1}{K_3 T'_{do}} & \frac{1}{T'_{do}} & 0 & 0 \\ -\frac{K_A K_5}{T_A} & 0 & -\frac{K_A K_6}{T_A} & -\frac{1}{T_A} & 0 & \frac{K_A}{T_A} \\ -\frac{K_1}{M} & -\frac{D}{M} & -\frac{K_2}{M} & 0 & -\frac{1}{T_w} & 0 \\ -\frac{K_c K_1 T_1}{M T_2} & -\frac{K_c D T_1}{M T_2} & -\frac{K_c K_2 T_1}{M T_2} & 0 & \frac{K_c}{T_2}\left(1-\frac{T_1}{T_w}\right) & -\frac{1}{T_2} \end{bmatrix} \quad (6)$$

$$[B] = \begin{bmatrix} 0 \\ \frac{\Delta T}{M} \\ 0 \\ 0 \\ 0 \\ 0 \end{bmatrix} \quad (7)$$

$$[C_1] = [1 \quad 0 \quad 0 \quad 0 \quad 0 \quad 0] \quad (8)$$

$$[C_2] = [0 \quad 1 \quad 0 \quad 0 \quad 0 \quad 0] \quad (9)$$

The parameters of each component of the SMIB system are presented in Tables 1 to 5 below.

**Table 1: Generator Parameter Data**

| Parameter | M | D | $\acute{T}_{do}$ | $x_d$ | $\acute{x}_d$ | $x_q$ |
|---|---|---|---|---|---|---|
| Value | 9,26 | 0 | 7,76 | 0,973 | 0,19 | 0,55 |

**Table 2: Operational Condition Data**

| Parameter | P | Q | $\lvert v_{t0} \rvert$ | $f$ |
|---|---|---|---|---|
| Value | 0,9545 | 0,2757 | 1,0311 | 60 |

**Table 3: Transmission Line Data**

| Parameter | R | X | G | B |
|---|---|---|---|---|
| Value | 0,034 | 0,997 | 0,249 | 0,262 |

**Table 4: Excitation Data**

| Parameter | $K_A$ | $T_A$ |
|---|---|---|
| Value | 50 | 0,05 |

**Table 5: SMIB Constant Data**

| Parameter | K1 | K2 | K3 | K4 | K5 | K6 |
|---|---|---|---|---|---|---|
| Value | 0,3383 | 1,1491 | 0,6550 | 0,5469 | -0,0961 | 0,8389 |

Subsequently, the state-space equations of the SMIB system are derived using the obtained values, allowing the transfer function of the SMIB system to be determined. In this study, the transfer function is obtained using MATLAB software. The parameters of the Power System Stabilizer (PSS) used in the SMIB system are presented in Table 6 below.

**Tabel 6: Nilai-Nilai Parameter PSS**

| Parameter | Value |
|---|---|
| $K_c$ | 9,81082 |
| $T_1$ | 0,42613 |
| $T_2$ | 0,1000 |

The parameter data from Table 6 above are subsequently substituted to obtain the Eigen values of the SMIB system. The results are then compared with the PSS parameters optimized using the BSA method, with the optimization limits provided in Table 7 below.

**Table 7: The optimization limit values**

| Parameter | Value |
|---|---|
| $K_c$ | $1{,}0000 \leq K_c \leq 50{,}0000$ |
| $T_1$ | $0{,}0100 \leq T_1 \leq 1{,}0000$ |
| $T_2$ | $0{,}0010 \leq T_2 \leq 0{,}2000$ |

***Backtracking Search Algorithm***

The backtracking search methodology use iteration and trial parameters to determine the optimal value of SMIB with PSS. The parameters and iterations of the optimization are presented in Table 8 below.

**Table 8: Optimization Parameter**

| Parameter | Value |
|---|---|
| N | 50 |
| Iteration | 1000 |
| Number of trials | 10 |

The backtracking search algorithm comprises five primary stages: initialization, selection I, mutation, crossover, and selection II. Figure 2 illustrates the flowchart depicting the steps of the backtracking search algorithm employed in this investigation.

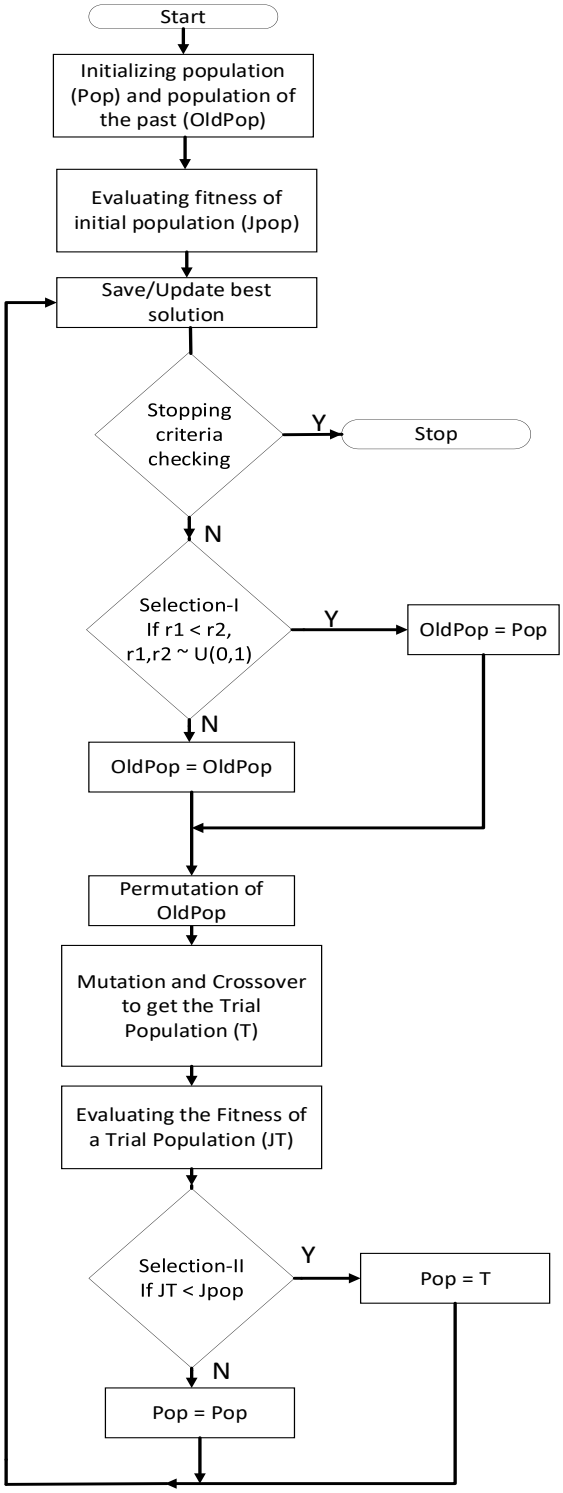


**Figure 2: The stage of BSA optimization**

The algorithm commences with the implementation of an initialization procedure. During this preliminary phase, the system generates a set of 50 initial populations (denoted as Pop), consisting of random values for Kc, T1, and T2. Subsequently, the previous population, referred to as OldPop, is also established, generating 50 values for each of Kc, T1, and T2. Following the formation of the initial population, the system initiates an exploration of the objective function by searching for the minimum zeta value. This minimum zeta is obtained using the eigenvalue matrix, where the smallest zeta value is retained and iteratively processed throughout the model's iterations. After

this, the system evaluates the stopping criteria. If the criteria are met, specifically if the number of iterations has reached the predefined maximum threshold, the process terminates. Otherwise, if the stopping condition is not yet satisfied, the process proceeds to the next phase.

In the subsequent step, the system engages in Selection-I, where two stochastic values ($r_1$ and $r_2$) are compared. If $r_1$ is found to be less than $r_2$—implying that the values of Kc, T1, and T2 derived from each zeta value in the previous population (OldPop) are lower—these values are updated to align with those of the current population (Pop). Otherwise, the previous population remains unchanged and continues to be used. Next, a permutation step is executed to introduce new variations into the population.

Following the completion of Selection-I, the algorithm proceeds to the mutation and crossover stage. During this phase, novel solutions are generated by modifying individuals from the historical population through the application of mutation and crossover operators. The mutation process aims to explore unmapped regions of the solution space by leveraging information from the historical population, with the objective of identifying superior individuals. The crossover process combines the mutated solutions with original ones to exploit and evaluate potentially optimal combinations through recombination. The outcome of this phase is a newly formed experimental population, denoted as T. This population includes the three parameters Kc , T1, and T2, each carefully adjusted within predefined parameter bounds. Once the experimental population T is established, the system re-evaluates the damping ratio (zeta) values within it. These evaluation results are then used in Selection-II, during which the current population (Pop) is updated. If the fitness of the experimental population surpasses that of the current one—indicated by a higher fitness value—the current population is updated to reflect the experimental one (Pop = T). If not, the previous values are retained. This iterative process continues, returning to the stopping criterion assessment, and loops until the termination condition is satisfied. Upon completion of the algorithm, the optimal solution identified throughout the process is designated as the final output.

In this research, frequency domain analysis was conducted for the open-loop transfer function, the closed-loop transfer function, and robustness evaluation. The frequency domain analysis of the open-loop transfer function focused on assessing the gain margin and phase margin. For the closed-loop transfer function, the analysis emphasized the examination of bandwidth and resonance peak. Furthermore, the robustness analysis involved evaluating the peak sensitivity and peak complementary sensitivity. The design criteria employed for the analysis of rotor angle and angular speed are presented in Tables 9 and 10.

**Table 9: Design Criteria – Rotor Angle**

| Analysis | Design Criteria | Value |
|---|---|---|
| Open-Loop Frequency Domain | Gain Margin (dB) | > 6 |
| | Phase Margin (degrees) | $30^o < \gamma < 60^o$ |
| Closed-Loop Frequency Domain | Bandwidth (rad/s) | > 7,1082 |
| | Resonance Peak | $1,0 < M_r < 1,5$ |
| Robustness | Peak Sensitivity Value | < 2 |
| | Peak Complementary Sensitivity Value | < 1,25 |

**Table 10: Design Criteria – Rotor Angular Speed**

| Analysis | Design Criteria | Value |
|---|---|---|
| Open-Loop Frequency Domain | Gain Margin (dB) | > 6 |
| | Phase Margin (degrees) | $30^o < \gamma < 60^o$ |
| Closed-Loop Frequency Domain | Bandwidth (rad/s) | Inf |
| | Resonance Peak | $1,0 < M_r < 1,5$ |
| Robustness | Peak Sensitivity Value | < 2 |
| | Peak Complementary Sensitivity Value | < 1,25 |

## 3. Results and discussion

The objective function's variation from the BSA method is illustrated in Figure 3, which is a result of the ten experiments consisting 1000 iterations where each iteration used 50 data points.

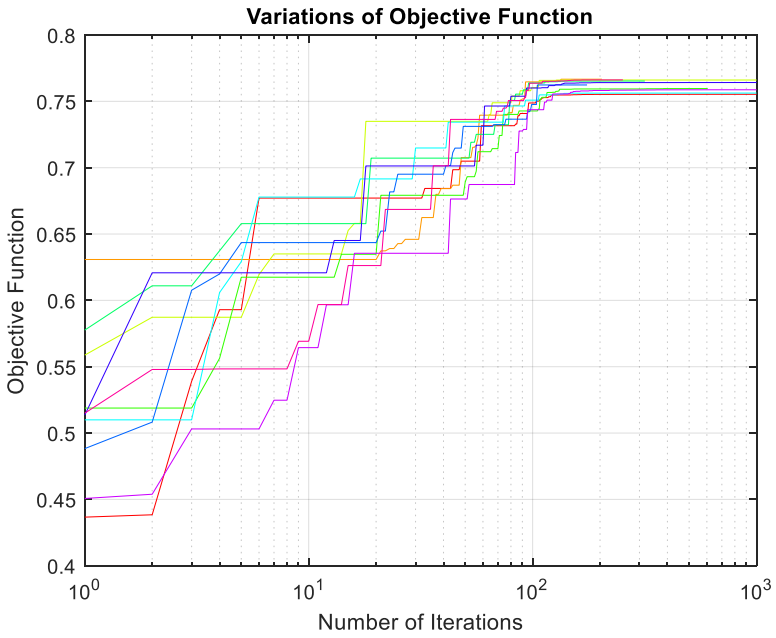


**Figure 3: Variation of the Objective Function**

The optimal damping ratio/zeta was obtained from each experiment. The data of the optimal values for each experiment are presented in Table 11.

**Table 11: Optimal Value Data**

| Zeta | Kc | T1 | T2 |
|---|---|---|---|
| 0,7637 | 38,2095 | 0,1026 | 0,0014 |
| 0,7621 | 38,1957 | 0,1031 | 0,0015 |
| 0,7569 | 38,0601 | 0,1043 | 0,0023 |
| 0,7637 | 38,2582 | 0,1027 | 0,0011 |
| 0,7606 | 38,2571 | 0,1036 | 0,0012 |
| **0,7649** | **38,1845** | **0,1022** | **0,0015** |
| 0,7502 | 38,2899 | 0,1069 | 0,0012 |
| 0,7621 | 38,0425 | 0,1028 | 0,0023 |
| 0,7647 | 38,1339 | 0,1022 | 0,0018 |
| 0,7485 | 38,2525 | 0,1074 | 0,0015 |

The table 11 indicates that the damping/zeta has a maximum value of 0.7649. This occurs when the parameters used are Kc of 38.1845, T1 of 0.1022 seconds and T2 of 0.0015 seconds. These parameters were obtained with a computation time of 37.802566 seconds.

**Table 12: Frequency Domain Analysis Information for Open-Loop and Closed-Loop Transfer Functions of SMIB – Rotor Angle.**

| Parameter | Values | | |
|---|---|---|---|
| | Without PSS | With PSS | PSS+BSA |
| Gain Margin (dB) | Inf | 27,9560 | Inf |
| Phase Margin (degrees) | −44,4840 | Inf | 89,5440 |
| Bandwidth (rad/s) | 7,1082 | 0,9148 | 2,6605 |
| Resonance Peak Value | 1,4104 | 0,9625 | 0,7937 |

Table 12 presents the parameters derived from the frequency domain analysis simulations of the open-loop transfer function, both with and without the Power System Stabilizer (PSS) prior to optimization. The gain margin changed from infinite dB to 27.9560 dB, an increase of 6 dB, which meets the design criteria. The phase margin changed from −44.4840° to Inf°, which does not meet the design criteria. The system without PSS demonstrated instability, as indicated by the negative phase margin. In contrast, the system with PSS showed a significant improvement in margin, providing strong stability. However, the gain margin remained unchanged, still infinite dB, both before and after the PSS optimization. The phase margin changed from −44.4840° to 89.5440°, but this still does not meet the design criteria. The BSA optimization caused a drastic shift from negative to positive phase, which enhances the system's stability.

Additionally, from Table 12, it can also be seen that the bandwidth parameter changes from 7.1082 rad/second to 0.9148 rad/second. The peak resonance value changes from 1.4104 to 0.9625. The system with PSS diminishes both the bandwidth and the peak resonance value. Theoretically, a wider bandwidth results in a faster system response. The system without PSS has satisfied the design criteria requirements, despite the bandwidth being at the threshold limit. The bandwidth parameter of the optimized PSS is 2.6605 rad/s. This indicates a reduction in bandwidth, signifying non-compliance with the design parameters that necessitate a bandwidth exceeding that of the system prior to the application of a stabilizer. The PSS system utilizing BSA optimization diminishes bandwidth, resulting in a sluggish system response. The peak resonance value shifts from 1.4104 to 0.7937, indicating that the system, prior to the implementation of PSS, adheres to the design criterion, which stipulates a range of 1 to 1.5. Post-PSS implementation, the system exhibits a resonance peak value below unity, signifying an overdamped response. The subsequent illustration depicts the Bode diagram for the open-loop transfer function alongside the Bode magnitude diagram for the closed-loop transfer function.

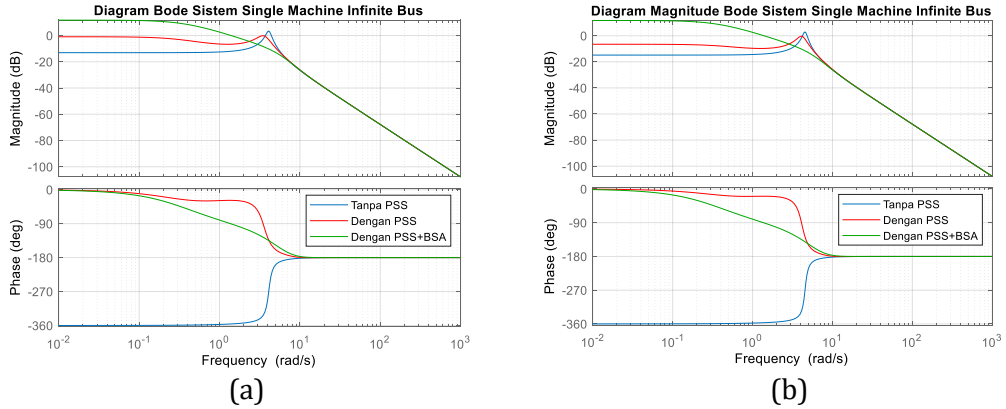


(a) (b)

**Figure 4: Frequency Domain Analysis of the Open-Loop Transfer Function – Rotor Angle (a), Frequency Domain Analysis of the Closed-Loop Transfer Function - Rotor Angle (b)**

**Table 13: Frequency Domain Analysis Information for Open-Loop and Closed-Loop Transfer Functions of SMIB – Rotor Angular Speed.**

| Parameter | Values | | |
|---|---|---|---|
| | Without PSS | With PSS | PSS+BSA |
| Gain Margin (dB) | 35,8680 | Inf | Inf |
| Phase Margin (degrees) | Inf | Inf | Inf |
| Bandwidth (rad/s) | Inf | Inf | Inf |
| Resonance Peak Value | 0,0164 | 0,0092 | 0,0037 |

The simulation results of the frequency domain analysis for both open-loop and closed-loop transfer functions are presented in Table 13. The gain margin parameter increased from 35.8680 dB to infinity dB, in accordance with the design criteria, which is greater than 6 dB. The phase margin remained constant at infinity, both without and with the PSS. However, based on the data above, the system is stable in the third configuration, and the basic system (without PSS) has shown good stability. An infinite gain margin suggests maximum possible system stability. The phase margin also remained unchanged before and after PSS optimization, with both configurations maintaining an infinite degree, indicating robust phase stability. Analysis results indicate that neither system satisfies the design criteria.

The bandwidth parameter remains unchanged, remaining infinite both before and after PSS. Both satisfy the design criteria, specifically, infinite, indicating that theoretically, the system reaction is accelerating. The peak resonance value diminishes with the application of PSS, decreasing from 0.0164 to 0.0092 before and after PSS optimization. Similar to the previous discussion regarding rotor angle, the system, upon the introduction of PSS, will diminish the peak resonance value, hence enhancing the damping characteristics. Bandwidth does not change either without or after the PSS optimization. Both show infinite rad/second, thus indicating the system's fast response capacity. Peak resonance value parameter decreases from 0.0164 to 0.0037. The peak resonance value of the system with the BSA-optimized PSS has decreased significantly, around 77% of the system without PSS. Both exhibit small values, indicating effective damping and minimum oscillation. The subsequent illustration depicts a Bode diagram for an open-loop transfer function alongside a Bode magnitude diagram for a closed-loop transfer function.

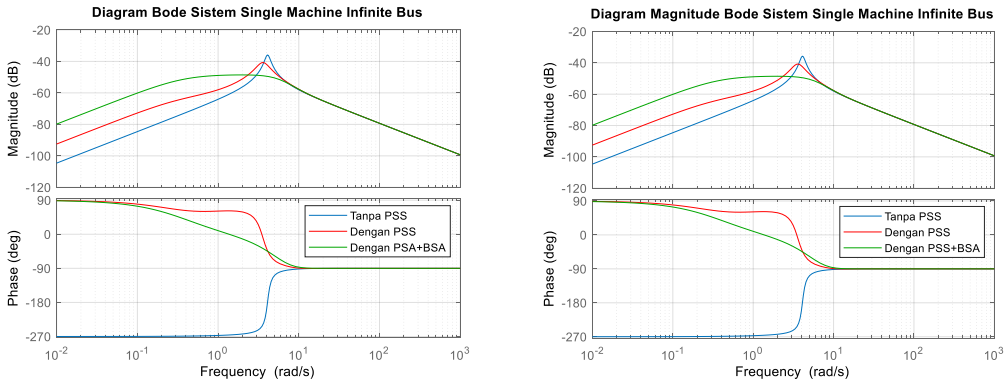


(a) (b)

**Figure 5: Frequency Domain Analysis of the Open-Loop Transfer Function – Rotor Angular Speed (a), Frequency Domain Analysis of the Closed-Loop Transfer Function - Rotor Angular Speed (b)**

**Table 14: Results of Frequency Domain Analysis on Systems that Meet the Design Criteria – Rotor Angle**

| Parameter | Gain Margin (dB) | Phase Margin (degrees) | Bandwidth (rad/s) | Resonance Peak Value |
|---|---|---|---|---|
| Without PSS | ✓ | × | × | ✓ |
| PSS | ✓ | × | × | × |
| PSS +BSA | ✓ | × | × | × |

Based on the predetermined rotor angle design criteria, the frequency domain analysis indicates that none of the three systems including SMIB system without PSS, with a PSS, and with a PSS optimized using BSA algorithm—fully satisfy the design requirements for both open-loop and closed-loop transfer functions. The gain margin in each system meets the required design thresholds, indicating a robust level of stability against gain variations. However, the resonant peak criterion is only fulfilled by the system without PSS, with a value approaching the upper limit of 1.4104, while the other systems show progressively lower values. This suggests that both PSS-equipped systems, whether optimized or not, are effective in reducing the resonant peak magnitude. On the other hand, none of the systems meet the required bandwidth criterion, implying that the inclusion of a PSS, even when optimized using BSA, does not significantly enhance the system's response speed.

**Table 15: Frequency Domain Analysis Results of Systems that Meet the Design Criteria – Rotor angular speed**

| Parameter | Gain Margin (dB) | Phase Margin (degrees) | Bandwidth (rad/s) | Resonance Peak Value |
|---|---|---|---|---|
| Without PSS | ✓ | × | × | × |
| PSS | ✓ | × | ✓ | × |
| PSS +BSA | ✓ | × | ✓ | × |

According to the predetermined design criteria for rotor angular speed, none of the three systems including SMIB system without PSS, with a PSS, and with a PSS optimized using BSA algorithm—satisfy the frequency domain design requirements for both open-loop and closed-loop transfer functions. While the gain margin of each system meets the design specifications, none of the systems fulfill the required phase margin criteria. A high gain margin indicates strong system stability in response to gain variations. However, in terms of bandwidth, both PSS-equipped systems—whether optimized with BSA or not—meet the design criteria. The analysis of rotor angular speed further demonstrates that the systems with PSS exhibit good stability and a fast system response time.

Overall, the results of the frequency domain analysis of the Single Machine Infinite Bus (SMIB) system show that an increase in bandwidth corresponds to a decrease in rise time, peak time, and settling time, thereby leading to a faster system response. Conversely, a higher resonant peak indicates a greater overshoot, resulting in a more oscillatory system response. An increase in phase margin enhances system damping, thus improving overall system stability. The system incorporating a Power System Stabilizer (PSS) optimized using the Bacterial Swarm Algorithm (BSA) demonstrates a reduction in both bandwidth and resonant peak, while exhibiting an increase in phase

margin. Although this may slightly delay the rise time, the optimization emphasizes improved system stability.

In prior investigations conducted by Xiaodong Wang et al., the methodology employed was the Melnikov's method [22]. Utilizing this approach, it was determined that the method was effectively employed to ascertain the threshold for the initiation of chaotic motion. Computational simulations indicate that external perturbations and nonlinear damping exert a substantial impact on the nonlinear dynamic behavior exhibited by this system. Concurrently, within the framework of this study, the Backtracking Search Analysis method is employed to derive the maximum zeta value, which serves to dampen the system in order to enhance stability. However, it is noteworthy that the pursuit of increased stability necessitates a trade-off in terms of the speed and responsiveness of the system.

## 4. Conclusion

The analysis of the Single Machine Infinite Bus (SMIB) system reveals that the implementation of a Power System Stabilizer (PSS) optimized using the Backtracking Search Algorithm (BSA) significantly enhances system stability and robustness. In the absence of a PSS, the system exhibits critical instability, as evidenced by a negative phase margin of −44.4840° in rotor angle response and a sensitivity peak approaching the design limit at 1.9133, indicating a high risk of instability. However, the application of a BSA-optimized PSS markedly improves these characteristics, resulting in a substantial positive phase margin of 89.5440°, while maintaining an infinite gain margin.

A trade-off between system stability and dynamic performance is evident in the observed changes in rotor angle bandwidth. The system without a Power System Stabilizer (PSS) exhibits a bandwidth of 7.1082 rad/s, whereas the system employing a PSS optimized by the Backtracking Search Algorithm (BSA) reduces this value to 2.6605 rad/s. Additionally, the resonant peak decreases from 1.4104 to 0.7937, reflecting a shift from an underdamped to an overdamped response. This indicates an enhancement in system stability at the expense of a slower response. In terms of rotor speed control, although both configurations maintain an infinite bandwidth, the system with the BSA-optimized PSS demonstrates a significant reduction in the resonant peak (from 0.0164 to 0.0037), suggesting markedly improved damping characteristics. These changes underscore a fundamental control principle: enhancing stability often requires compromising system responsiveness and speed.

## Author contribution

Author 1 conceptualized the research, defined the hypotheses, and designed the study methodology including the data collection protocol and statistical analysis plan.

Author 2 responsible for data curation and ensuring that all data was accurately organized and formatted and wrote the original draft of the manuscript, including the results and discussion sections.

## Funding statement

This research received no specific grant from any funding agency in the public, commercial, or not-for-profit sectors.

## Acknowledgements

The authors ould like to express gratitude for the support provided by the Department of Electrical Engineering and the Faculty of Engineering at Andalas University in the implementation of this research.

## Competing interest

The authors declare that they have no competing interests

## References

[1] Y. Kirange and P. Nema, "A Survey on Improving Power System Dynamic Stability with a Single Machine Infinite Bus," in *2023 International Conference for Advancement in Technology (ICONAT)*, 2023, pp. 1–8. doi: 10.1109/ICONAT57137.2023.10080028.

[2] G. Gonzalez-Avalos, G. Ayala-Jaimes, N. B. Gallegos, and A. P. Garcia, "Modeling and Simulation of an Integrated Synchronous Generator Connected to an Infinite Bus through a Transmission Line in Bond Graph," *Symmetry (Basel)*, vol. 16, no. 10, p. 1335, Oct. 2024, doi: 10.3390/sym16101335.

[3] G. Gonzalez-Avalos and G. Ayala-Jaimes, "Modelling and Simulation of a Synchronous Generator Connected to Infinite Bus in a Bond Graph Approach," in *2024 28th International Conference on Methods and Models in Automation and Robotics (MMAR)*, 2024, pp. 346–351. doi: 10.1109/MMAR62187.2024.10680814.

[4] Y. K. Kirange and P. Nema, "Innovative Approach to Enhance Stability: Neural Network Control and Aquila Optimization Integration in Single Machine Infinite Bus Systems," *Advances in Technology Innovation*, vol. 9, no. 2, pp. 99–115, 2024, doi: 10.46604/aiti.2024.13360.

[5] M. Ruswandi Djalal *et al.*, "Analisis Pemasangan Power System Stabilizer Pada Single Machine Infinite Bus Untuk Kondisi Variasi Beban," 2022.

[6] H. Q. Nguyen, D. N. Nguyen, and L. Q. Vinh, "Design of power system stabilizers based on the model of single machine infinite bus power system," *Journal of Science and Technology - HaUI*, vol. 60, no. 5, May 2024, doi: 10.57001/huih5804.2024.155.

[7] V. Q. Vinh, D. N. Nguyen, H. Q. Nguyen, and V. T. Ha, "Using the Single Machine Infinite Bus Power System Model to Design Power System Stabilizers," in *2023 Asia Meeting on Environment and Electrical Engineering (EEE-AM)*, 2023, pp. 1–5. doi: 10.1109/EEE-AM58328.2023.10395334.

[8] M. A. Prakasa and I. Robandi, "Power System Stabilizer Tuning Improvement for Single-Machine Infinite Bus using Equilibrium Optimizer Algorithm," in *2022 International Seminar on Intelligent Technology and Its Applications (ISITIA)*, 2022, pp. 320–325. doi: 10.1109/ISITIA56226.2022.9855203.

[9] Y. Zhu *et al.*, "Configuration method of PSS lead-lag compensator parameters," in *E3S Web of Conferences*, EDP Sciences, Jan. 2021. doi: 10.1051/e3sconf/202123301059.

[10] H. Wang, H. Wang, P. Xin, and Z. Song, "Frequency Domain Stability Analysis and Simulation of New Energy Power Generation Systems," in *2024 9th Asia Conference on Power and Electrical Engineering (ACPEE)*, 2024, pp. 933–937. doi: 10.1109/ACPEE60788.2024.10532689.

[11] C. R. Shah, M. Molinas, S. Føyen, S. D'Arco, R. Nilsen, and M. Amin, "Single Coordinate Bode Plots for Stability Evaluation of MIMO Power Electronics Systems via a Frequency Coupling Corrective Factor," Nov. 21, 2024. doi: 10.36227/techrxiv.173220610.07636645/v1.

[12] Y. Song, D. J. Hill, and T. Liu, "Network-based analysis of rotor angle stability of power systems," *Foundations and Trends in Electric Energy Systems*, vol. 4, no. 3, pp. 222–345, Nov. 2020, doi: 10.1561/3100000011.

[13] A. A. Sallam and O. P. Malik, *Power System Stability: Modelling, Analysis and Control*. The Institution of Engineering and Technology, 2015. doi: 10.1049/PBPO076E.

[14] N. Vieyra, E. Rodríguez-Monzón, P. Maya-Ortiz, and C. Angeles-Camacho, "An Output-Feedback Controller For a Single Machine Infinite Bus Power System," 2023.

[15] S. Salhi, A. Necira, A. Salhi, D. Benkhetta, and D. Naimi, "Optimal control design for power system stabilizer using a novel crow search algorithm dynamic approach," *STUDIES IN ENGINEERING AND EXACT SCIENCES*, vol. 5, no. 2, p. e9782, Oct. 2024, doi: 10.54021/seesv5n2-397.

[16] S. Paul, S. Sultana, P. K. Roy, P. K. Burnwal, D. Sengupta, and N. Dey, "Optimal Tuning of Single Input Power System Stabilizer Using Chaotic Quasi-Oppositional Differential Search Algorithm," in *Control Applications in Modern Power Systems*, S. Kumar, M. Tripathy, and P. Jena, Eds., Singapore: Springer Nature Singapore, 2024, pp. 133–147.

[17] Z. Sun, Y. Cao, Z. Wen, Y. Song, and Z. Sun, "A Grey Wolf Optimizer algorithm based fuzzy logic power system stabilizer for single machine infinite bus system," *Energy Reports*, vol. 9, pp. 847–853, 2023, doi: https://doi.org/10.1016/j.egyr.2023.04.365.

[18] K. M. Din, F. Daqaq, and R. Ellaia, "Backtracking Search Algorithm with Lemur Optimizer for Numerical and Global Optimization," in *2024 10th International Conference on Optimization and Applications (ICOA)*, 2024, pp. 1–6. doi: 10.1109/ICOA62581.2024.10754131.

[19] M. Arab and W. Fadel, "Optimal Reactive Power Flow of AC-DC Power System with Shunt Capacitors Using Backtracking Search Algorithm," *Energies (Basel)*, vol. 17, no. 3, Feb. 2024, doi: 10.3390/en17030749.

[20] Y. L. Ekinci, Ç. Balkaya, and G. Göktürkler, "Backtracking Search Optimization: A Novel Global Optimization Algorithm for the Inversion of Gravity Anomalies," *Pure Appl Geophys*, vol. 178, no. 11, pp. 4507–4527, 2021, doi: 10.1007/s00024-021-02855-3.

[21] M. A. Z. Raja *et al.*, "Evolutionary backtracking search optimization for the dynamics of nonlinear benchmark physical systems," *Waves in Random and Complex Media*, pp. 1–26, Jun. 2023, doi: 10.1080/17455030.2023.2226249.

[22] X. Wang, Y. Chen, G. Han, and C. Song, "Nonlinear dynamic analysis of a single-machine infinite-bus power system," Appl Math Model, vol. 39, no. 10–11, pp. 2951–2961, 2015, doi: 10.1016/j.apm.2014.11.018.